DOI: https://doi.org/10.1016/j.seppur.2018.11.034

PREPRINT VERSION

Calcite buffer effects in electrokinetic remediation of clopyralid-polluted soils

López-Vizcaíno, R. [a,c,*,1], dos Santos, E.V[b]., Yustres, A.[c], Rodrigo, M.A.[d], Navarro, V.[c], Martínez-Huitle, C.A.[a]

[a] Institute of Chemistry, Federal University of Rio Grande do Norte, Campus Universitario, 59078-970 Natal, Brazil.

[b] School of Science and Technology, Federal University of Rio Grande do Norte, Campus Universitario, 59078-970 Natal, Brazil.

[c] Geoenvironmental Group, Civil Engineering School, University of Castilla-La Mancha, Avda. Camilo José Cela s/n, 13071 Ciudad Real, Spain.

[d] Department of Chemical Engineering, Faculty of Chemical Sciences & Technologies, University of Castilla-La Mancha, Campus Universitario s/n, 13071 Ciudad Real, Spain.

*** Corresponding author,** Rubén López-Vizcaíno, ruben.lopezvizcaino@uclm.es // r.lopezvizcaino@gmail.com.

[1]**Permanent address** of Rubén López-Vizcaíno is Geoenvironmental Group, Civil Engineering School, University of Castilla-La Mancha, Avda. Camilo José Cela s/n, 13071 Ciudad Real, Spain.

ABSTRACT

This work presents a study of the dissolution-precipitation processes of calcite in soil undergoing electrokinetic remediation processes. For this purpose, a numerical inspection of one of these processes in a calcareous soil (10% calcite content) contaminated with an of the organochlorine acid herbicide (3,6-dichloro-2-pyridinecarboxylic acid) was carried out. The numerical tool used to perform this analysis was the Multiphysics for EKR (M4EKR), a module programmed by the authors in the COMSOL Multiphysics platform. A detailed analysis of the pH, the distribution of species that have a significant influence on soil buffering capacity (carbonates and calcite), as well as the pollutant, has been performed. In this way, the kinetics of the calcite dissolution-precipitation processes have been analysed in order to determine the pH of the water in the pores and, therefore, how it directly affects the effectiveness of the treatment. Additionally, a sensitivity analysis of the selected EKR process has been carried out at different values of the rate of calcite dissolution due to the uncertainty associated with the reactive surface area parameter.

KEYWORDS

Electrokinetic soil remediation, Multiphysics simulation, soil buffering capacity, herbicide, M4EKR, calcite

1. INTRODUCTION

The application of an electrical potential gradient between electrodes located in a soil activates a series of electrokinetic transport mechanisms capable of mobilising water (electroosmosis), ionic species (electromigration) and even charged particles (electrophoresis). Specifically, this technique is called electrokinetic remediation (EKR) when it is applied to contaminated soils with the aim of mobilizing polluting species to controlled extraction points [1-4]. The coupling of the above-mentioned transport mechanisms and the fact that, these treatments can be successfully applied in soils with low hydraulic permeability, where Darcy flow is very limited, makes EKR technology a very versatile technique and consequently, an efficient and competitive alternative for treating pollution events with different compounds such as heavy metals [5-8], PAH [9-13] or pesticides [14-18].

Regarding the EKR processes, the electrolysis of water is also an important electrochemical reaction developed on the electrode surface. This process simultaneously generates high concentrations of protons (H^+) by the oxidation reaction of water on the anodic surface and hydroxyl ions (OH^-) in the cathodic reduction reaction. The changes in the concentration of H^+ and OH^- are reflected in the generation of an important pH gradient in the soil located between anodes and cathodes.

The pH changes generated in the vicinity of the electrodes depend on the amount of electro-generated H^+ and OH^- and, in turn, on the electrical potential gradient applied in the process. However, the pH-variations observed in the rest of the domain are determined by the mobility of the acidic and alkaline fronts, from the anodic and cathodic zones respectively. The transport of the pH front is mainly due to the electromigratory flow of H^+ and OH^- species to the opposite sign electrodes and advective/diffusive processes, all of which are strongly influenced by soil buffering capacity [19-24]. Generally, soil

buffering capacity is defined by the contribution of different processes: (i) protonation/deprotonation of substances present in the porewater, (ii) adsorption/desorption and ion exchange between the soil and the porewater and (iii) dissolution-precipitation of minerals [25].

At this point it is important to stress the importance of pH changes in EKR treatments. This variable directly influences the chemical speciation of the substances present in soil and porewater, conditioning their ionic nature. Consequently, the pH of the system can determine the predominant mechanism of transport of chemical species in the soil.

In order to have a global understanding of the evolution of pH in an EKR process, it is necessary to improve the knowledge of the interactions attained between the electrokinetic transport phenomena and the physical, chemical and electrochemical processes that take place in an EKR treatment. The main objective of this work is to evaluate the influence of soil buffering capacity on the performance of an EKR process. For this purpose, a numerical analysis of the EKR treatment of a calcareous soil with a calcite content of 10%, contaminated with clopyralid (3,6-dichloro-2-pyridinecarboxylic acid, a common acid herbicide) was performed. Specifically, this study has evaluated the effects generated by the calcite dissolution-precipitation processes on the general behaviour of the EKR process and their importance for a better understanding of this type of treatment.

The numerical tool used was the M4EKR module, Multiphysics for EKR [26]. M4EKR is a numerical model developed by the authors as a result of the knowledge gained over the last years in the treatment of contaminated soils using electrokinetic techniques [27-35]. The M4EKR model has been implemented in COMSOL Multiphysics and is capable of simulating the general behaviour trends of an EKR process by solving a coupled

problem of reactive transport and electric field. This makes the M4EKR module a powerful computational tool that has been used to carry out different studies [36-38].

In this work, an assessment of the spatial distribution of the concentration of the species that have a significant influence on soil buffering capacity (carbonates and calcite) was performed. The relationship between the observed behaviour and the pH profiles obtained is also analysed, as well as the direct influence on the performance of the simulated EKR process. Additionally, and due to the difficulties in accurately predicting the kinetics of calcite dissolution-precipitation, associated with the uncertainty of the reactive surface area [39], a sensitivity analysis of the selected EKR process was performed using different values of this parameter, which is equivalent to different levels of the rate of calcite dissolution. Consequently, this study provides useful information on the influence of soil buffer capacity on the general performance of an EKR process applied to the decontamination of a calcareous soil with acidic contaminants.

2. CONCEPTUAL MODEL AND NUMERICAL IMPLEMENTATION

M4EKR is a reactive transport model applied to unsaturated porous media. It is a very flexible numerical tool. Its adaptability and capacity for gradual implementation of improvements are easy by the fact that the base module has been programmed in a multiphysical environment. [26].

For conceptual simplification, the M4EKR version employed in this work does not consider gas transport and the deformability of the soil. Due to the small scale of the simulated tests (laboratory scale), it is acceptable to assume isothermal conditions (298 K). Given these simplifications, it is clear that the model will not perfectly match the actual behaviour in an EKR process. However, this is not a limitation in the scope of the work, since the aim is to improve phenomenological understanding and not to replicate a

real case. Soil buffering capacity is provided by: chemical reactions with proton consumption/production (see Table 4), and dissolution-precipitation of calcite [40]. The adsorption/desorption processes onto the soil were not consider. As a novelty, the M4EKR version used in this work has been improved with the implementation of a kinetic model of calcite dissolution/precipitation, extrapolable to any other mineral if present.

Appendix A presents the basic mathematical formulation employed in module M4EKR. A more detailed description of the formulation can be found in literature [26].

2.1. Calcite mass balance

The evolution of the mass of calcite is obtained solving the mass balance equation

$$\frac{dM_{calcite}}{dt} = R_{calcite} \qquad \text{Eq. (1)}$$

where $M_{calcite}$ is the total mass of calcite (mol/m^3) and $R_{calcite}$ is the calcite production/consumption rate (mol m^{-3} s^{-1}).

2.2. Kinetic of calcite precipitation/dissolution

The calcite production/consumption rate, $R_{calcite}$ (mol m^{-3}·s^{-1}), has been estimated by a general equation provided by Lasaga [41]:

$$R_{calcite} = \pm k_{calcite} \cdot \phi \cdot Sr \cdot \rho_w \cdot S_{calcite} \cdot \left(1 - \Omega_{calcite}^{\theta}\right)^{\eta} \qquad \text{Eq. (2)}$$

where $k_{calcite}$ is the kinetic constant (mol s^{-1}m^{-2}) of dissolution (negative value) or precipitation (positive value) processes, $S_{calcite}$ is the reactive surface area (m^2 kg$^{-1}_{H_2O}$), and $\Omega_{calcite}$ is the saturation ratio. Finally, θ and η are empirical parameters that determine the relation between reaction rate and saturation ratio. The parameters selected for calcite were θ = 0.5 and η = 2 [42]. A reference value for $S_{calcite}$ was extracted from literature [42]. The parameters ϕ, Sr and ρ_w correspond to the soil porosity, saturation degree and

water density. The saturation ratio ($\Omega_{calcite}$) is estimated using the Eq. (3) where $K_{s,\ calcite}$ is the solubility constant of calcite [43] and IAP is the ionic activity product, calculated as indicated in Eq. (4) where $a_{Ca^{+2}}$ and $a_{CO_3^{-2}}$ are the activities of Ca^{2+} y CO_3^{2-} respectively.

$$\Omega_{calcite} = \frac{IAP_{calcite}}{K_s,calcite} \quad \text{Eq. (3)}$$

$$IAP_{calcite} = a_{Ca^{2+}} \cdot a_{CO_3^{2-}} \quad \text{Eq. (4)}$$

The kinetic constant ($k_{calcite}$) has been defined using a model that takes into account the influence additional mechanisms in the value of $k_{calcite}$. In this case, a dependence on the activity HCO_3^- has been observed for carbonate minerals such as calcite [42]. The expression for $k_{calcite}$ reads as follows

$$k_{calcite} = k_{25}^{calcite} \cdot exp\left[\frac{-E_a^{calcite}}{R}\left(\frac{1}{T} - \frac{1}{298.15}\right)\right] + k_{25}^{HCO_3^-} \cdot exp\left[\frac{-E_a^{HCO_3^-}}{R}\left(\frac{1}{T} - \frac{1}{298.15}\right)\right] \cdot \left(a_{HCO_3^-}\right)^{n_{HCO_3^-}}$$

Eq. (5)

where E_a^i and a_i are the activation energy (kJ mol^{-1}) and the activity, and k_{25}^i and n_i are a model parameters for the species considered, in this particular case the mineral considered (calcite) and HCO_3^-. Table 1 shows the numerical values of parameters for the kinetic model selected [42].

Table 1. Kinetic model parameters from calcite

Parameters	Units	Values
$k_{25}^{calcite}$	mol m^{-2} s^{-1}	$1.8 \cdot 10^{-7}$
$k_{25}^{HCO_3^-}$	mol m^{-2} s^{-1}	$1.9 \cdot 10^{-3}$
$E_a^{calcite}$	kJ mol^{-1}	66
$E_a^{HCO_3^-}$	kJ mol^{-1}	67
$n_{HCO_3^-}$	-	1.63
θ	-	0.5
η	-	2
$S_{calcite}$	m^2 $kg_{H_2O}^{-1}$	1.54

3. NUMERICAL IMPLEMENTATION

The M4EKR model was implemented in COMSOL Multiphysics [44], a partial differential equation solver developed in a multiphysics environment. COMSOL uses the finite element method with Lagrange multipliers. One of its most remarkable attributes is its versatility, since the user has great freedom to define the system of equations required to solve the selected case [45-47].

M4EKR solves transport problems coupled with chemical speciation using a monolithic approach, without using any other external software. This strategy optimises the resources and reduces the computational cost. This aspect is of high importance and provides a novelty to this work because it is common to use operator-splitting procedures for solving reactive transport problems [48-50]. Furthermore, the computational capacity of the M4EKR module goes beyond this kind of codes since it also allows to solve simultaneously the partial differential equations that define the transport and balance of mass of water, mass of dissolved species and electric charge, (See Appendix A, Eqs. A.1, A.9 and A.10 respectively), the ordinary differential equations used to solve the mass

balance in electrolyte wells, (Eq. A.11) and the algebraic equations from the stoichiometric approach used in the chemical speciation.

4. SIMULATION OF THE EKR PROCESS

4.1. Modelled configuration

4.1.1. Polluted Soil

The electrokinetic remediation of a polluted soil with an organochlorine herbicide (20 mg of clopyralid $kg^{-1}_{dry\,soil}$) was analysed. The selected soil is a calcareous soil, (calcite mass fraction 10%). Table 2 presents the textural and mineralogical properties of the modelled soil. The soil parameters are show in Table 3. Bulk density and gravimetric water content are representative of the natural state of this soil [30].

Table 2. Textural and mineralogical properties of the modelled soil.

Mineralogical Analysis	
Mineral	**%**
Quartz	9
Feldspar	12
Calcite	10
Kaolinite	23
Smectite	25
Illite	21
Textural Parameters	
Size fraction	**%**
Sand	26.1
Silt	68.6
Clay	5.3

Table 3. Modelled soil parameters.

Parameters	Description	Values	Units
α_{VG}	Parameter of the Van Genuchten[51] retention curve	0.0147	kPa^{-1}
n_{VG}	Parameter of the Van Genuchten[51] retention curve	1.2593	-
m_{VG}	Parameter of the Van Genuchten[51] retention curve	0.2059	-
ϕ	Porosity	0.4681	-
K_{sat}^{h}	Saturated hydraulic permeability	2.03×10^{-10}	$m\ s^{-1}$
K_{sat}^{eo}	Saturated electroosmotic permeability	2.4×10^{-9}	$m^2\ V^{-1}\ s^{-1}$
ρ_s	Soil particle density	2681.5	$kg\ m^{-3}$
ρ_{bulk}	Bulk density	1894.4	$kg\ m^{-3}$
w	Moisture	0.32	$kg_{water}\ kg_{dry\ soil}^{-1}$
δ_i^L	Longitudinal dispersivity of species *i*	0.01	m
τ	Vapour tortuosity	1.00	-

4.1.2. Porewater

The geochemical model implemented consists of 7 components and 20 secondary species. The chemical reactions and thermodynamic properties (equilibrium constants [43], hard-core diameters and diffusion coefficients) are presented in Table 4. The activity coefficients of the species were estimated by WATEQ Debye-Hückel model [52].

Table 4. Thermodynamic properties of the modelled geochemical systems

	Species	Reactions	log K_i^{eq} (25ºC)	Hard core diameter / Å	D_i^o / m^2s^{-1}
Components	Cl^-	Cl^-	0	3.6	2.03×10^{-9}
	H_2O	H_2O	0	3.4	5.27×10^{-9}
	H^+	H^+	0	4.1	9.31×10^{-9}
	CO_3^{-2}	CO_3^{-2}	0	4.7	9.55×10^{-10}
	Ca^{+2}	Ca^{+2}	0	5.7	7.93×10^{-10}
	Na^+	Na^+	0	4.1	1.33×10^{-9}
	$Clopy^-$	$Clopy^-$	0	3.6	$8.20\times10^{-10*}$
Secondary species	OH^-	$H_2O \leftrightarrow OH^- + H^+$	-14	3.6	5.27×10^{-9}
	HCO_3^-	$CO_3^{-2} + H^+ \leftrightarrow HCO_3^-$	10.33	3.6	1.18×10^{-9}
	H_2CO_3	$CO_3^{-2} + 2H^+ \leftrightarrow H_2CO_3$	16.68	3.4	1.92×10^{-9}
	$CaHCO_3^+$	$Ca^{+2} + CO_3^{-2} + H^+ \leftrightarrow CaHCO_3^+$	11.43	4.1	5.06×10^{-10}
	$CaCO_3$	$Ca^{+2} + CO_3^{-2} \leftrightarrow CaCO_3$	3.22	3.4	4.46×10^{-10}
	$Ca(OH)^+$	$Ca^{+2} + H_2O \leftrightarrow Ca(OH)^+ + H^+$	-12.78	4.1	$2.13\times10^{-10*}$
	$NaHCO_3$	$Na^+ + HCO_3^- \leftrightarrow NaHCO_3$	10.08	3.4	6.73×10^{-10}
	$NaCO_3^-$	$Na^+ + CO_3^{-2} \leftrightarrow NaCO_3^-$	1.27	3.6	5.85×10^{-10}
	NaOH	$Na^+ + H_2O \leftrightarrow NaOH + H^+$	-14.75	3.4	$1.89\times10^{-10*}$
	$CaCl^+$	$Ca^{+2} + Cl^- \leftrightarrow CaCl^+$	-0.29	4.1	$2.13\times10^{-10*}$
	NaCl	$Na^+ + Cl^- \leftrightarrow NaCl$	-0.5	3.4	$1.89\times10^{-10*}$
	$CaCl_2$	$Ca^{+2} + 2\ Cl^- \leftrightarrow CaCl_2$	-0.64	3.4	7.54×10^{-10}
	$Clopy^-$	$Clopy^- + H^+ \leftrightarrow Clopy$	2.32	3.4	$8.20\times10^{-10*}$
Solid species	Calcite	$Calcite \leftrightarrow Ca^{+2} + CO_3^{-2}$	-8.48**	-	-

* Obtained by using Pikal´s model [53].
** Solubility product of calcite [43].

3.1.3. Modelled Experimental setup

The experimental setup modelled was a lab-scale EKR reactor. This setup is composed of an electrokinetic cell divided in three compartments: the anolyte compartment(AC), the catholyte compartment (CC), where electrodes are located and with dimensions 15×3×3 cm, and a central compartment destined to place the polluted soil with a capacity of 675 ml (LWH: 15×15×3 cm). The level of electrolyte in compartments is constant during the tests by adding anolyte through gravity and extracting the catholyte by overflow of the CC. This modelled experimental setup has been outlined in detail in

preceding studies [26, 36, 37]. Fig. 1 shows a scheme of the conceptual model of the setup simulated.

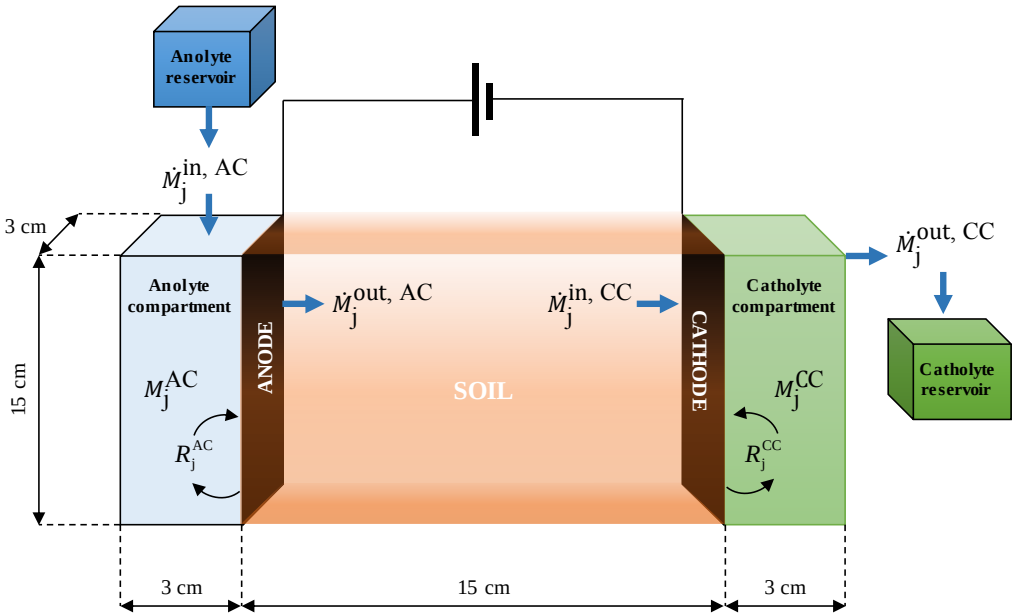

Figure 1. Conceptual model of the one-dimensional domain proposed for simulation. Symbols described in Appendix A.

This setup defines a one-dimensional (1D) configuration that allows reducing the computational time and provides easily interpretable results needed to understand the EKR main trends.

3.1.4. Initial conditions

The initial mass fraction of calcite in the soil was 10%. The initial electrolytes (anolyte and catholyte) are an aqueous solution of $CaCO_3$ and NaCl equilibrated with the calcite present in the soil. The same solution with an amount of clopyralid equivalent to 20 mg $\mathrm{kg}_{\mathrm{dry\,soil}}^{-1}$ is considered as initial porewater. The electrolyte added to the AC during the EKR test is an aqueous NaCl solution with the same pH as the initial porewater. Table 5 shows the chemical initial conditions of the different solutions used in the study.

Table 5. Chemical **i**nitial conditions.

	Total components concentration / m						pH	Ionic Strength / m
	H^+	Na^+	Ca^{2+}	CO_3^{2-}	Cl^-	$Clopy_{anion}$		
Soil porewater	3.41×10^{-3}	3.58×10^{-3}	2.49×10^{-3}	3.12×10^{-3}	5.36×10^{-3}	3.67×10^{-4}	7.25	1.10×10^{-2}
Inital electrolyte	3.41×10^{-3}	3.58×10^{-3}	2.49×10^{-3}	3.12×10^{-3}	5.75×10^{-3}	0	7.25	1.10×10^{-2}
Addition to anolyte reservoir	-1.32×10^{-7}	3.58×10^{-3}	0	0	3.57×10^{-3}	0	7.25	3.57×10^{-3}

Initially, the electrolyte compartments are filled completely and they are open to atmosphere, therefore the initial liquid pressure, P_L, is equal to 100 kPa (atmosphere pressure). The initial condition was an electric potential gradient equal to zero.

3.1.5. Boundary conditions

To solve the problem presented in this work it is necessary to define three types of boundary conditions for each of the balances presented: electrical, hydraulic and mass of dissolved chemical species. For the first case, an average electrical potential gradient of 1 V cm^{-1} was applied. In the case of water mass balance, the boundary condition with the initial condition (P_L = 100 kPa) since the compartments are open to the atmosphere and maintain a constant level during all the cases evaluated. The boundary condition used in the mass balances of chemical species was imposed by the concentration of components in the electrolyte compartments. It is important to note that the definition of this type of boundary condition is obtained in a coupled form by means of the resolution of J-2 ordinary differential equations defining the mass balance of the chemical components in the electrolyte wells. (See Appendix A, Eq. A.11).

3.2. Simulation of EKR tests

3.2.1. Effect of calcite dissolution-precipitation process in EKR behaviour.

In this section, the importance of calcite dissolution-precipitation processes in the performance of an EKR process has been evaluated. To this end, two EKR processes have been studied: (i) the treatment of the described soil contaminated with clopyralid, in which the dissolution-precipitation processes of this mineral have been taken into account (Mineral Reaction test, MR-test) and (ii) an EKR process equivalent to the first case, in which it has been assumed that there are no precipitation-dissolution processes of calcite (no Mineral Reaction test, nMR-test). This strategy has been selected to determine the effect of these reactions on the overall performance and behaviour of the selected EKR process.

Figure 2 shows the spatial distribution of the pH in both tests for different observation times (0, 1, 2, 24 and 48 h).

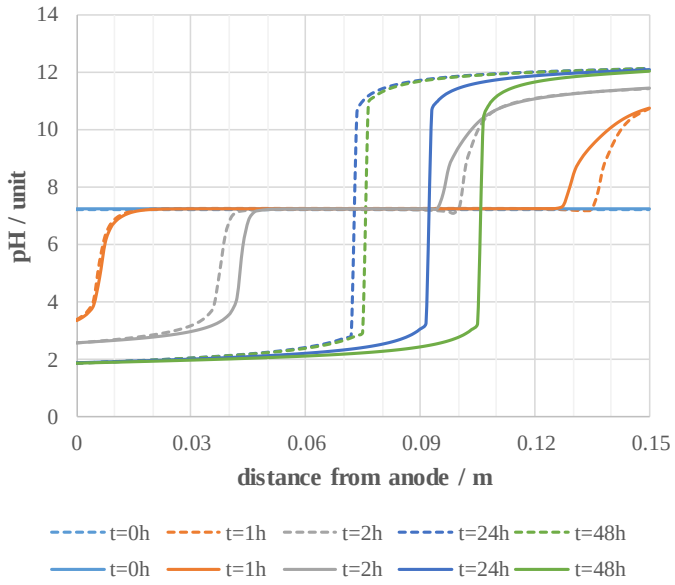

Figure 2. pH spatial distribution at selected times. MR-test, dashed line; nMR-test, solid line.

In both tests, the pH distribution observed in the domain is characteristic of EKR treated soil. At short times (1 h), the generation of a pH gradient between the anodic (pH=3.5) and cathodic (pH=10.5) zones due to the generation of H^+ in the AC and OH^- in the CC through the electrolysis of water is already observed. The transport of these ionic species through the soil generates an acidic pH front (to the cathode) and an alkaline pH front (to the anode) that collide at a point where the pH gradient is maximum. The location of this point will be very important in the discussion of results, the Maximum pH Gradient Point (MpHGP). It can be seen how the velocity with which the pH fronts move is different in the two numerical tests evaluated. The rate of advance of the acidic front is slower in the case of MR-test. This decrease is more significant at higher test times. It can be seen that after 48 hours of testing the acidic front has spread over 10.5 cm of the domain in the nMR-test, and only 7.5 cm in the MR-test. This behaviour suggests that the MR-test involves additional processes that act as a pH buffer such as the dissolution of calcite [54]. The spatial distribution of the calcite content in the MR-test is shown in Fig. 3. It is important to note that initially the calcite content is in equilibrium with the calcium carbonate concentration.

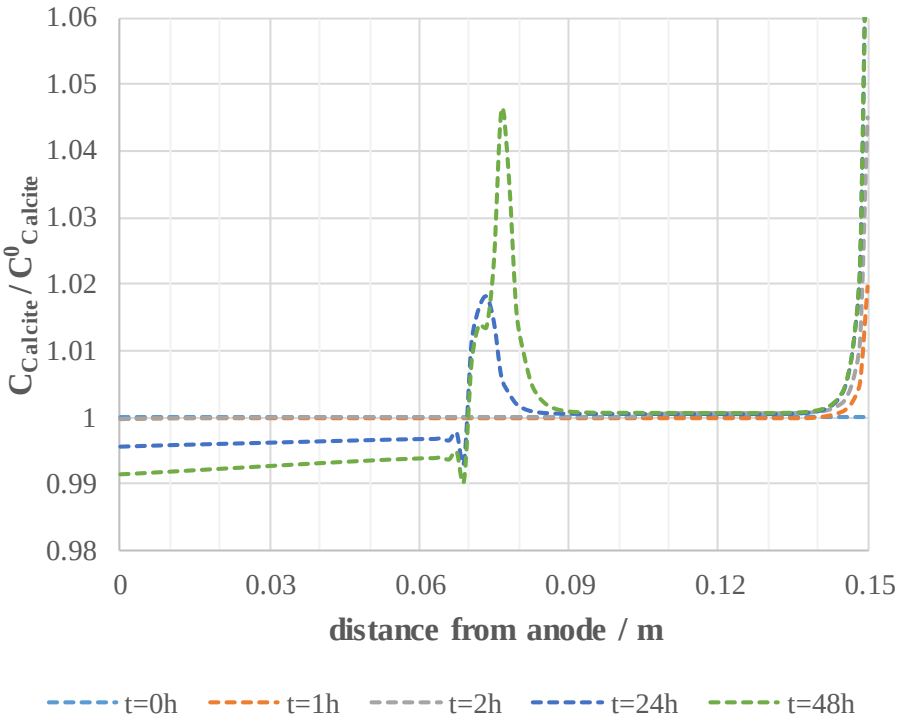

281

282 **Figure 3.** Spatial distribution of normalized calcite content at selected times in MR-test.

283 On the other hand, when the content of calcite in the soil is analysed, three areas with
284 different behaviour can be identified. In the zone with acidic pH, between AC and
285 MpHGP, a decrease in the initial calcite content of the soil is observed, accentuating in
286 the zone immediately adjacent to MpHGP. The calcite dissolution process is active under
287 these conditions, and this trend is most noticeable at higher test times (24 and 48 h)
288 because these processes have been simulated by means of a chemical kinetic process and
289 not by a chemical equilibrium. Meanwhile, in the soil-CC interface zone (where the
290 cathode is located) a sudden increase in the calcite content generated by the precipitation
291 can be seen. This behaviour has been observed (Fig. 4) in previous experimental work
292 [55].

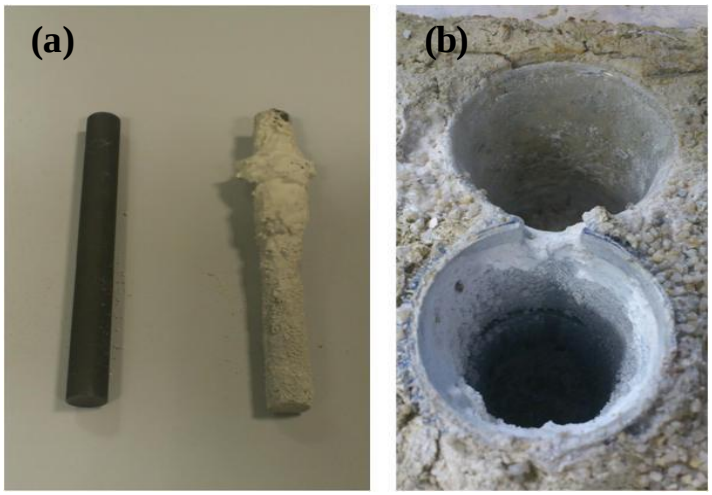

293

294 **Figure 4.** Evidences of mineral precipitation on (a) cathode before EKR and (b) CC.

295 The third zone which was identified corresponds to the domain close to the MpHGP
296 where the acidic and alkaline pH fronts (maximum pH gradient) are located. In this area
297 there is an accumulation of calcite. In both the second and third zones, the observed
298 calcite precipitation is limited only to very localize areas and not to the entire soil domain
299 with basic pH, as would be expected. In order to understand more precisely the processes
300 of calcite dissolution-precipitation observed in Figure 3, it is necessary to analyze the
301 chemical speciation of the carbonate system. For this purpose, the spatial distribution of
302 the concentration of the carbonate species ($H_2CO_3^{\circ}$, HCO_3^-, CO_3^{-2} y Ca^{2+}) is shown in Fig.
303 5.

304

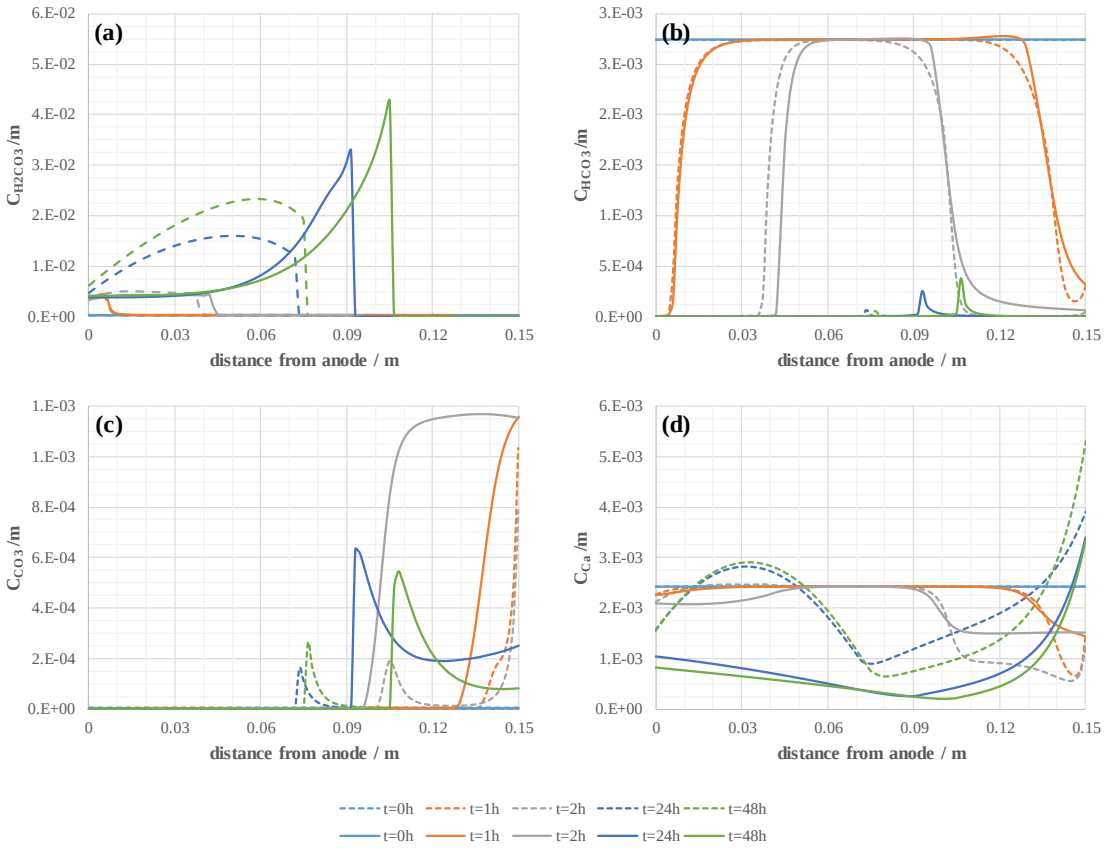

305

306 **Figure 5.** Spatial distribution of species concentration at selected times. MR-test, dashed line;
307 nMR-test, solid line. (a) $H_2CO_3^\circ$, (b) HCO_3^-, (c) CO_3^{-2} and (d) Ca^{2+}.

308 Fig. 5a shows the distribution of $H_2CO_3^\circ$ (species including the sum of the concentrations
309 of H_2CO_3 and dissolved CO_2) in the domain. A common trend is observed in both
310 numerical tests, the accumulation of this species in the post-MpHGP area. This can be
311 explained taking into account that this species is only present in systems with pH highly
312 acid. In addition, taking into account the transport features, this species has a neutral
313 charge, so the predominant transport mechanisms are the advective flux (hydraulic and
314 electro-osmotic flow) and the diffusive/dispersive processes with a net flux from anode
315 to cathode [26]. However, if we compare the spatial distributions at the same observation
316 times, we can see how there are notable differences between the two tests analysed. In
317 the MR-test it is observed the $H_2CO_3^\circ$ is present in a smaller volume of soil, which
318 indicates that there is a relationship between the concentration of $H_2CO_3^\circ$ and the process

of dissolution of calcite. As Plummer demonstrated [39], this process takes place through simultaneous reactions (See Eq.5-9).

$$CaCO_3 + H^+ \leftrightharpoons Ca^{2+} + HCO_3^- \quad \text{Eq.(6)}$$

$$CO_3^{2-} + 2H^+ \leftrightharpoons H_2CO_3^\circ \quad \text{Eq.(7)}$$

$$CaCO_3 + H_2CO_3^\circ \leftrightharpoons Ca^{2+} + 2HCO_3^- \quad \text{Eq.(8)}$$

$$CaCO_3 + H_2O \leftrightharpoons Ca^{2+} + HCO_3^- + OH^- \leftrightharpoons Ca^{2+} + CO_3^- + H_2O \quad \text{Eq.(9)}$$

The progression of these reactions depends directly on the pH of the system and therefore on the chemical speciation of the carbonate system. [56]. In systems with strongly acidic pHs, the Eq.6 and Eq.7 reactions become important. Taking into account this reactivity, the consumption of H^+ produced by the water electrolysis could justify the slowing down observed in the MR-test of the acidic front (See Fig. 2), the reduction of the calcite content by dissolution (See Fig. 3) and the increase in the concentration of H_2CO_3 and accumulation in the area after the acidic front (See Fig. 5a). In addition, the decrease of the calcite content in the left side of the MpHGP point could be explained if it is known that the predominant reaction of the calcite solution is the Eq.6 reaction and if it is taken into account that for pH greater than 5 and with a partial pressure of CO2 greater than 0.1 atm, Eq.8 becomes important. With the contribution of the latter reaction to the general process of dissolution, the change in shape of the spatial distribution of H_2CO_3 mentioned above can be satisfactorily described.

The second carbonate species analysed was the bicarbonate ion, HCO_3^- (Fig. 5b). This species exists at pH values between 6.3 and 10.25. For this reason, HCO_3^- is present in significant amounts only in the initial stage of the test (1 and 2 h), when the pH fronts are not very abrupt. The ion carbonate, CO_3^{-2}, exhibits the opposite behavior to $H_2CO_3^\circ$. The

342 CO_3^{-2} is predominantly presents in the right side of the MpHGP and has negative charge
343 as well as HCO_3^-. Both species are predominantly transported by electromigration to the
344 anode. These clarifications could explain the spatial distribution of the concentration of
345 these species and the accumulation observed behind the MpHGP (See Fig. 5b and 5c).
346 Quantitatively, the MR-test presents a lower accumulation of both CO_3^{-2} and HCO_3^- in the
347 area near the MpHGP since these species are, together with Ca^{2+} (See reaction R.9), the
348 drivers of the generation of calcite by precipitation (See Fig.3). This behaviour is also
349 observed in the area of the soil-CC interface, even at short test times (1 and 2h). This
350 suggests that the precipitation process is faster than the dissolution process, as there is no
351 decrease in calcite content at those times. In order to check this fact, the dimensionless
352 reaction rate $R^*_{calcite}$ has been evaluated as a function of the saturation ratio, $\Omega_{calcite}$ using
353 the expression (10) and giving the results in Figure 6.

354 $$R^*_{calcite} =\cdot \left(1 - \Omega^{\theta}_{calcite}\right)^{\eta} \qquad \text{Eq. (10)}$$

355 and giving the results in Figure 6.

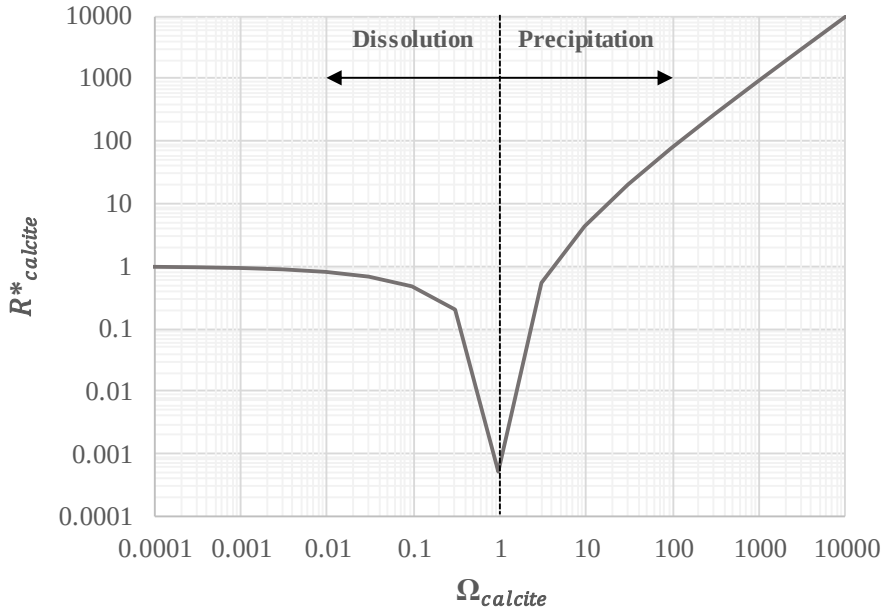

356

357 **Figure 6.** Influence of saturation ratio in dimensionless reaction rate.

Starting from a system in equilibrium ($\Omega_{calcite}$=1), it can be observed that a decrease of $\Omega_{calcite}$ activates the process of dissolution of calcite. The rate of the calcite dissolution process has an increasing trend corresponding to the decrease of the $\Omega_{calcite}$. This evolution continues until it reaches a point where the reaction rate is stabilized at a constant value. This implies that from this point on, the dependence of the reaction rate of the dissolution process with $\Omega_{calcite}$. is negligible. Meanwhile, the precipitation process occurs when $\Omega_{calcite}$ is greater than 1. The evolution of the precipitation reaction rate as a function of $\Omega_{calcite}$ is entirely different. A roughly double log-linear increase is observed with the increase in the saturation ratio. This indicates that the precipitation rate is proportional to the concentration of species involved in that reaction (See reaction Eq.8). In this line, from a quantitative point of view, it can be observed how changes in an order of magnitude in $\Omega_{calcite}$ are translated into much more significant changes in the reaction rate in the precipitation process. This would explain the rapid calcite deposition shown in Fig. 3. Finally, the spatial distribution of Ca^{2+} ion is analysed (Fig. 5d). Both tests show an accumulation of this species in the area of the CC, mainly due to the contribution of the electromigration process to the net transport of this ion [26]. The most noticeable difference between the two tests analysed is the increase in concentration observed in the acidic zone (after MpHGP) in the MR-test. This trend is according with the process of calcite dissolution observed in this zone.

Subsequently, the influence of the buffer effect generated by the dissolution of calcite on the speciation and transport of clopyralid was analysed. Two species have been considered, acid and anionic.

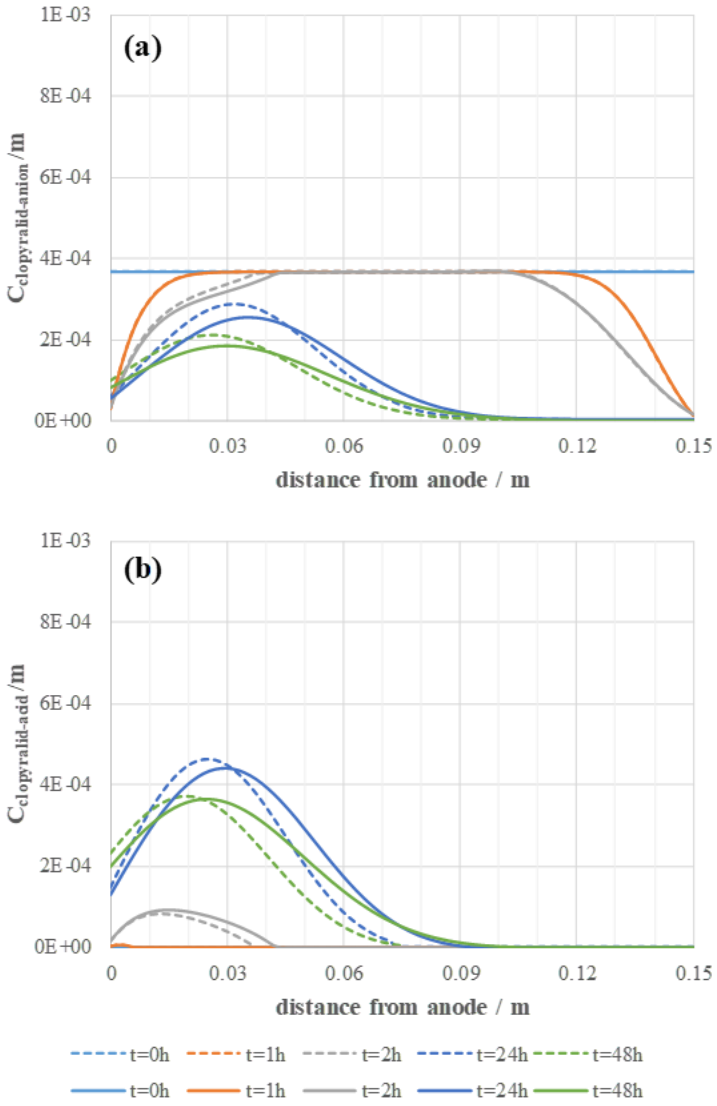

381

382 **Figure 7**. Spatial distribution of the total concentration of (a) $Clopyralid_{anion}$ species and (b)
383 $Clopyralid_{acid}$ species at selected times. MR-test, dashed line; nMR-test, solid line.

384

385 The pH of the soil pore water affects the chemical speciation of the substances contained
386 in the soil [22, 57], so acidic species are present in the low pH soil zone, generally between
387 CA and MpHGP in EKR processes. In the case studied, $Clopyralid_{acid}$ species are
388 concentrated in this zone, favouring the transport of these species to the anodic
389 compartment mainly by diffusion [36]. Furthermore, $Clopyralid_{anion}$ species, in
390 equilibrium with acidic species, also accumulate in this zone and is susceptible to being

391 moved towards the anodic compartment mainly by electromigration [36]. For these
392 reasons, the performance of the EKR treatment of soils with this type of pollutant (acid
393 pollutant with anionic dissociation) improves when the volume of the acid soil zone is
394 reduced as has been proven in previous works [36]. The buffer effect generated by the
395 dissolution of calcite produces a reduction of the acidic zone. This is how it can be seen
396 in Fig 7. Fig 7 shows in those locations where an accumulation of contaminant is observed
397 (in one of the two species considered) it is always shown to a lesser extent in the MR-
398 test.

399 **3.2.2. Sensitivity analysis of reactive surface area in EKR behaviour.**

400 The buffer capacity of the soil depends directly on the precipitation/dissolution kinetics
401 of calcite, however, as previously discussed in the introduction, it is considerably
402 complex to accurately to estimate the kinetics due to the high uncertainty associated with
403 the reactive surface area [39]. For this reason, a sensitivity analysis of the simulated EKR
404 process has been carried out for different values of this parameter. For this purpose, three
405 additional MR-tests have been simulated in which a reactive surface area ($S_{calcite}$) value
406 of 3.08, 10 y 100 m^2 $kg^{-1}_{H_2O}$ (compared to the 1.54 used in the case analysed in section
407 3.2.1), has been assumed. The main results obtained in this study are shown in Fig. 8.

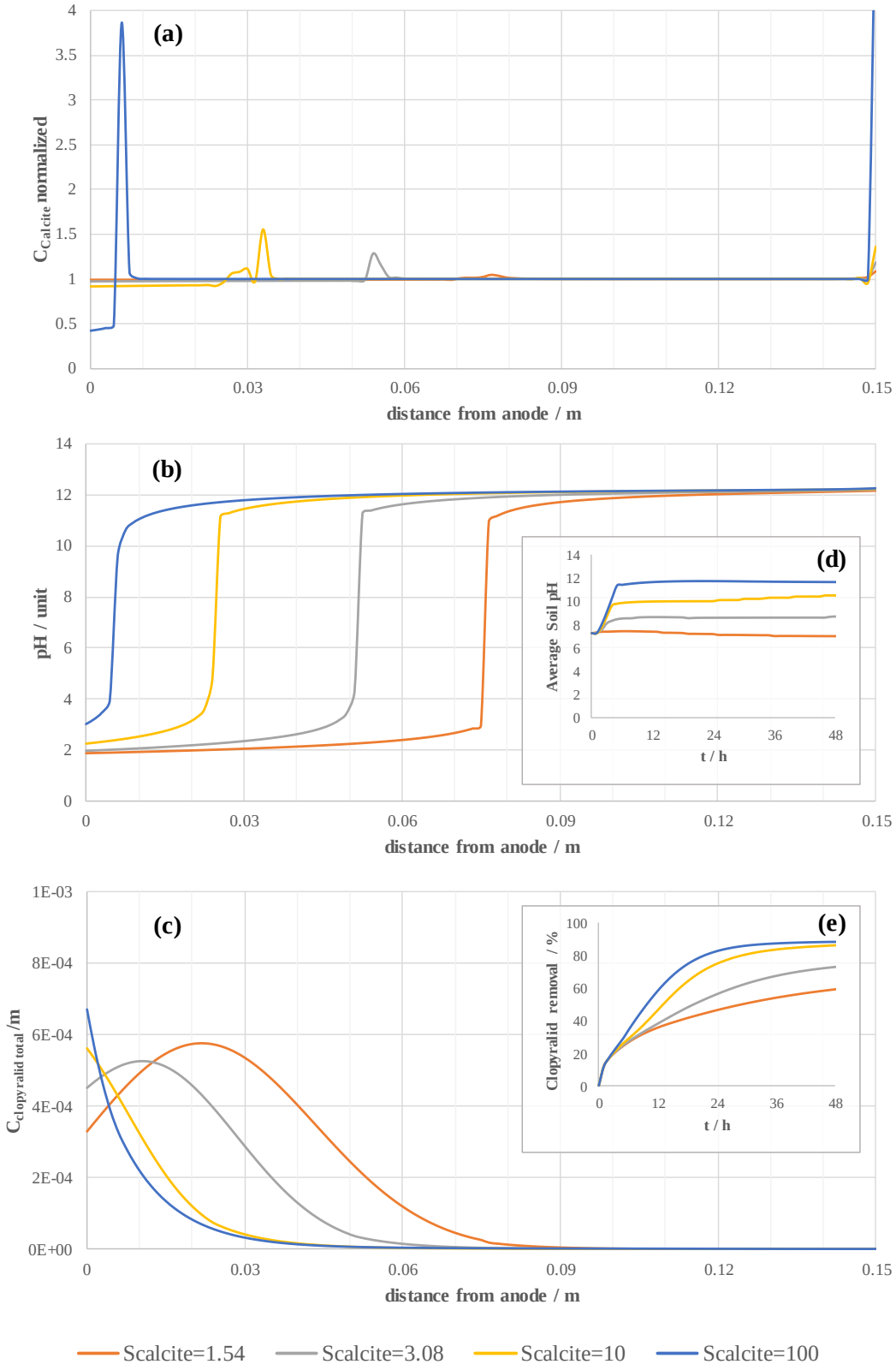

408

409 **Figure 8**. Sensitivity analysis of reactive surface area. Spatial distribution of the (a) of normalized
410 calcite content, (b) pH and (c) total concentration of Clopyralid species in soil at time test of 48
411 h. Dynamic response of the (d) average soil pH and (e) Clopyralid removal.

From a kinetic point of view, an increase in the value of $S_{calcite}$ translates into an increase in the rate at which the dissolution and precipitation processes of calcite take place. However, qualitatively, no significant influence is found. This can be verified by analysing Fig. 8a. The behaviour observed in the cases studied is common; the same three previously identified areas with active calcite reactivity are shown (Fig.3): (i) generalised dissolution in the acidic zone and punctual precipitation close to (ii) MpHGP and (iii) cathode. The extent to which these reactions develop is directly related to the $S_{calcite}$ value used.

Additionally, if the calcite dissolution process is specifically analyzed for a value of $S_{calcite}$ =100, a decrease in the mineral content of the soil is observed and therefore the consumption of H^+ is more pronounced This statement is in accordance with the pH profiles obtained in the MR-tests (Fig 8.b). It can be seen that as $S_{calcite}$, increases, and therefore the kinetics of calcite dissolution, the speed of the acidic front slows down. In order to be able to evaluate the buffer capacity of the soil in global terms, the temporal evolution of the average pH has been analysed (Fig. 8d). The results obtained confirm that an increase in $S_{calcite}$ causes a significant improvement in soil buffer capacity. In the MR-test with $S_{calcite}$=100 an average pH value of 11.6 is obtained in 5 h of test, which means that in this case the acidic front is totally neutralized.

As discussed in the previous section, the pH of the porewater determines chemical speciation and, consequently, the distribution of chemical species within the soil. Therefore, the spatial distribution of the pollutant has been analysed (Fig. 8c). The neutralization of the acidic front favours the accumulation of the contaminant in the area close to the CA and therefore the transport to this compartment. An increase in the soil buffer capacity produces an improvement in the performance of the EKR process, reaching an elimination rate of close to 90% (Fig. 8e). Although these results cannot be

taken valid in any configuration and for any soil, the information obtained in this sensitivity study is valid to show how the soil buffer capacity strongly influences the net performance of an EKR treatment.

4. CONCLUSIONS

This paper presents a numerical study of the processes of dissolution-precipitation of calcite in soil contaminated with clopyralid (an herbicide of the organochlorine acid type) by using an EKR treatment. The influence of the soil buffer capacity (associated with the dissolution of calcite) on the overall performance of the remediation process is also studied. In addition, experimentally observed behaviours, such as rapid calcite precipitation in the cathode electrode and the compartment where it is located, have been identified in the simulations. Thanks to the speciation of the carbonate system, it has been possible to improve the relative understanding of the reactive transport of these chemical species.

In addition, the results obtained have highlighted the importance of considering the processes of dissolution-precipitation in an EKR treatment, since the distribution of the soil pH depends to a large extent on them. The pH of the soil porewater is a fundamental variable in EKR treatments as it directly influences the speciation of the contaminants (and other chemical species present) and indirectly determines the transport mechanisms involved in the elimination of these contaminants. In the cases evaluated, it has been proven that the buffer effect produces improvements in the overall performance of the EKR process. The reduction of the advance of the acidic front, it favours the accumulation of polluting species in the vicinity of the anodic compartment and can be eliminated by means of anionic species by electromigration and of the acidic species by diffusive flux.

All these conclusions have been confirmed after a sensitivity analysis in which it has been evaluated how changes in the kinetics of the calcite dissolution-precipitation process abruptly modify the buffer capacity of the soil and therefore strongly influence the performance of the treatment. Therefore, it is very important to define accurately the kinetic parameters (specifically, the reactive surface area) since the interpretation of the results as well as the previous design of experimental setups depends on their numerical values.

ACKNOWLEDGEMENTS

The authors acknowledge funding support from: (i) Ministerio de Economía, Industria y Competitividad from Spanish Goverment and the European Union through the project [CTM2016-76197-R (AEI/FEDER, UE)]; (ii) Junta de Comunidades de Castilla-La Mancha and the European Union through the project [SBPLY/17/180501/000488 (JCCM/FEDER, UE)] and Postdoctoral Grant [SBPLY/16/180501/000402] awarded to Dr. López-Vizcaíno; (iii) Conselho Nacional de Desenvolvimento Científico e Tecnológico through the projects [CNPq-430121/2016-4], [CNPq-465571/2014-0], [CNPq-446846/2014-7] and [CNPq-401519/2014-7]; and (iv) Fundação de Amparo à Pesquisa do Estado de São Paulo through the project [2014/50945-4].

APPENDIX A

A.1. Water mass balance

Eq. (A.1) show the expression that defines the water mass balance:

$$\frac{\partial m_{\mathrm{w}}}{\partial t} + \nabla \cdot \mathbf{l}_{\mathrm{w}} = 0 \qquad \text{Eq. (A.1)}$$

where m_{w} is the mass of water per unit total volume (kg m^{-3}), and it is defined as Eq (A.2), $\nabla\cdot$ is the divergence operator, and $\mathbf{l}_{\mathrm{w}}$ is the mass flux of water (kg m^{-2} s^{-1}).

$$m_{\mathrm{w}} = \phi \cdot Sr \cdot \rho_{\mathrm{w}} + \phi \cdot (1 - Sr) \cdot \rho_{v} \qquad \text{Eq. (A.2)}$$

where ϕ is the soil porosity, *Sr* is the degree of saturation of the soil defined by van Genuchten model [58], ρ_{w} and ρ_{v} are the liquid and vapour water density (kg m^{-3}) respectively. Vapour water density is estimated using the psychrometric equation, Eq (A.3) [59]:

$$\rho_{\mathrm{v}} = \rho_{\mathrm{v}}^{\mathrm{o}} \cdot exp\left(\frac{M_{\mathrm{w}} \cdot s}{\rho_{\mathrm{w}} \cdot R \cdot T}\right) \qquad \text{Eq. (A.3)}$$

where M_{w} is the water molar mass, T is absolute temperature and, *s* is the matric suction, assumed equal to the capillary one (osmotic suction is not considered).

Eq. (A.4) shows the expression to calculate the flux term $\mathbf{l}_{\mathrm{w}}$:

$$\mathbf{l}_{\mathrm{w}} = \mathbf{l}_{\mathrm{w}}^{\mathrm{h}} + \mathbf{l}_{\mathrm{w}}^{\mathrm{eo}} = \rho_{\mathrm{w}} \cdot \left(\mathbf{q}_{\mathrm{w}}^{\mathrm{h}} + \mathbf{q}_{\mathrm{w}}^{\mathrm{eo}}\right) = \rho_{\mathrm{w}} \cdot \mathbf{q}_{\mathrm{w}} \qquad \text{Eq. (A.4)}$$

Where $\mathbf{l}_{\mathrm{w}}^{\mathrm{h}}$ is the Darcian flux, and $\mathbf{l}_{\mathrm{w}}^{\mathrm{eo}}$ is the electroosmotic flux, estimated with the semi-empirical model of Helmholtz-Smoluchowski [60]. The hydraulic and electroosmotic volumetric fluxes are presented as $\mathbf{q}_{\mathrm{w}}^{\mathrm{h}}$ and $\mathbf{q}_{\mathrm{w}}^{\mathrm{eo}}$ (See Eq. (A.5) and (A.7) respectively).

$$\mathbf{q}_{\mathrm{w}}^{\mathrm{h}} = -K_{\mathrm{e}}^{\mathrm{h}} \cdot (\nabla P_{\mathrm{L}} + g \cdot \rho_{\mathrm{w}} \cdot \nabla z) \qquad \text{Eq. (A.5)}$$

$$K_{\mathrm{e}}^{\mathrm{h}} = K_{\mathrm{sat}}^{\mathrm{h}} \cdot k_{\mathrm{rel}} = K_{\mathrm{sat}}^{\mathrm{h}} \cdot Sr^3 \quad \text{Eq. (A.6)}$$

$$\mathbf{q}_{\mathrm{w}}^{\mathrm{eo}} = -K_{\mathrm{e}}^{\mathrm{eo}} \cdot \nabla E \quad \text{Eq. (A.7)}$$

$$K_{\mathrm{e}}^{\mathrm{eo}} = K_{\mathrm{sat}}^{\mathrm{eo}} \cdot k_{\mathrm{rel}} = K_{\mathrm{sat}}^{\mathrm{eo}} \cdot Sr^3 \quad \text{Eq. (A.8)}$$

where $K_{\mathrm{e}}^{\mathrm{h}}$ is the effective hydraulic permeability, which is calculated by Eq (A6), $K_{\mathrm{sat}}^{\mathrm{h}}$ is the saturated permeability and k_{rel} is relative permeability. $K_{\mathrm{e}}^{\mathrm{eo}}$ is the effective electro-osmotic permeability, which is estimated by Eq (A8), and $K_{\mathrm{sat}}^{\mathrm{eo}}$ is the saturated electro-osmotic permeability. Both relative permeability are calculated using a model Brooks and Corey [61] with an exponent of 3. Additionally, ∇ is the gradient differential operator, g is gravity, z is the vertical coordinate, E is the electric potential.

A.2. Reactive transport

The geochemical model implemented in M4EKR module contemplates J components which is capable of generating a sum of N chemical species for the chemical reactions system considered (See Table 4) [62]. Thus, to determine the total chemical composition of the system, it is necessary to calculate the total mass of each component j (j=1...J) using a general mass balance equation, Eq (A.9). However, it is not required to solve J mass balances, only *J-2* partial differential equations are necessary to compute, due to the mass of one of the components is obtained applying the electroneutrality condition and water mass is calculated by Eq. (A.1) .

$$\frac{\partial m_{\mathrm{j}}}{\partial t} + \nabla \cdot \mathbf{l}_{\mathrm{j}} = R_{\mathrm{j}} \quad \text{Eq. (A.9)}$$

where m_{j} is the total mass of component j per unit total volume (mol m^{-3}), $\mathbf{l}_{\mathrm{j}}$ is its total molar flux (mol m^{-2} s^{-1}) which is defined as the sum of the contributions of four transport processes: advective transport generated by (i) hydraulic, (ii) electroosmotic and (iii)

electromigration fluxes, and (iv) Fickian diffusive-dispersive transport; and R_j is its rate of production or consumption (mol m^{-3} s^{-1}). Only *J-2* partial differential equations are required to be resolved, due to the total mass of one of the components is computed after electroneutrality and the total mass of water is calculated by Eq. (A.1).

The resolution of the chemical speciation has been obtained applying a classical stoichiometric approach based on to solve a system of mass-balance and mass-action equations [63]. The general algorithm of this method has been described in detail in literature [52, 62, 64, 65], even so the explicit formulation utilized in M4EKR can be seen in previous works [26, 37].

A.3. Electric charge balance

The balance equation of the total electric charge is defined by the expression Eq. (A.10) assuming that the electroneutrality condition is fulfilled throughout the entire domain and the system the system is not able to accumulate electric charge.

$$\nabla \cdot \mathbf{i} = 0 \qquad \text{Eq. (A.10)}$$

where **i** is the total current density (A m^{-2}), which is estimated according Ohm's law [26, 66]. Rhoades [67] and Appelo [68] approaches are applying to calculated the apparent electrical conductivity of the soil and electrical conductivity of pore water respectively. The equations of these methods can be found in López-Vizcaíno et al. ([26].

A.4. Mass balance in electrolyte wells

The temporal evolution of the mass of the *J* components is obtained solving *J-2* balance equations, Eq. (A.11) in each electrolyte compartment. The "ideal continuous stirring tank reactors" assumption is supposed in both electrolyte compartments.

$$\frac{dM_j^*}{dt} = \dot{M}_j^{in,*} - \dot{M}_j^{out,*} + R_j^* \qquad \text{Eq. (A.11)}$$

where M_j^* is the total mass of component j (mol) and $\dot{M}_j$ denotes the mass flow of component j (mol s^{-1}), being an input flow (superscript *in*) or output flow (superscript *out*). Additionally, R_j^* is the production/consumption/ term (mol s^{-1}) linked to the electrochemical reactions (only water electrolysis). The superscript * indicates the kind of electrolyte compartment, which is AC or CC (anolyte or catholyte compartment respectively). The equations employed to estimate these variables can be found in a previous work [26, 36, 37].

REFERENCES

[1] Y.B. Acar, Principles of electrokinetic remediation, Environment Science Technology, 27 (1993) 2638-2647.

[2] Y.B. Acar, R.J. Gale, A.N. Alshawabkeh, R.E. Marks, S. Puppala, M. Bricka, R. Parker, Electrokinetic remediation: Basics and technology status, J. Hazard. Mater., 40 (1995) 117-137.

[3] J. Virkutyte, M. Sillanpaa, P. Latostenmaa, Electrokinetic soil remediation - critical overview, Sci. Total Environ., 289 (2002) 97-121.

[4] K.R. Reddy, C. Cameselle, Electrochemical Remediation Technologies for Polluted Soils, Sediments and Groundwater, John Wiley and Sons, 2009.

[5] D.H. Kim, B.G. Ryu, S.W. Park, C.I. Seo, K. Baek, Electrokinetic remediation of Zn and Ni-contaminated soil, J. Hazard. Mater., 165 (2009) 501-505.

[6] L.M. Ottosen, H.K. Hansen, A.B. Ribeiro, A. Villumsen, Removal of Cu, Pb and Zn in an applied electric field in calcareous and non-calcareous soils, J. Hazard. Mater., 85 (2001) 291-299.

[7] M. Mascia, S. Palmas, A.M. Polcaro, A. Vacca, A. Muntoni, Experimental study and mathematical model on remediation of Cd spiked kaolinite by electrokinetics, Electrochimica Acta, 52 (2007) 3360-3365.

[8] M. Zhou, J. Xu, S. Zhu, Y. Wang, H. Gao, Exchange electrode-electrokinetic remediation of Cr-contaminated soil using solar energy, Separation and Purification Technology, 190 (2018) 297-306.

[9] M. Pazos, E. Rosales, T. Alcántara, J. Gómez, M.A. Sanromán, Decontamination of soils containing PAHs by electroremediation: A review, J. Hazard. Mater., 177 (2010) 1-11.

[10] J.N. Hahladakis, N. Lekkas, A. Smponias, E. Gidarakos, Sequential application of chelating agents and innovative surfactants for the enhanced electroremediation of real sediments from toxic metals and PAHs, Chemosphere, 105 (2014) 44-52.

[11] E. Bocos, C. Fernández-Costas, M. Pazos, M.Á. Sanromán, Removal of PAHs and pesticides from polluted soils by enhanced electrokinetic-Fenton treatment, Chemosphere, 125 (2015) 168-174.

[12] E. Méndez, J.A. García, G. Hernández, S. Solís, F. Prieto, S. Pamukcu, E. Bustos, Study of electrochemical removal of phenanthrene in bentonite clay by physicochemical indicators, Separation and Purification Technology, (2018).

[13] I.M.V. Rocha, K.N.O. Silva, D.R. Silva, C.A. Martínez-Huitle, E.V. Santos, Coupling electrokinetic remediation with phytoremediation for depolluting soil with petroleum and the use of electrochemical technologies for treating the effluent generated, Separation and Purification Technology, (2018).

[14] A.B. Ribeiro, J.M. Rodriguez-Maroto, E.P. Mateus, H. Gomes, Removal of organic contaminants from soils by an electrokinetic process: the case of atrazine. Experimental and modeling, Chemosphere, 59 (2005) 1229-1239.

[15] A.B. Ribeiro, E.P. Mateus, J.M. Rodríguez-Maroto, Removal of organic contaminants from soils by an electrokinetic process: The case of molinate and bentazone. Experimental and modeling, Separation and Purification Technology, 79 (2011) 193-203.

[16] M.A. Rodrigo, N. Oturan, M.A. Oturan, Electrochemically assisted remediation of pesticides in soils and water: a review, Chemical reviews, 114 (2014) 8720-8745.

[17] E. Vieira dos Santos, C. Sáez, P. Cañizares, C.A. Martínez-Huitle, M.A. Rodrigo, Reversible electrokinetic adsorption barriers for the removal of atrazine and oxyfluorfen from spiked soils, J. Hazard. Mater., 322 (2017) 413-420.

[18] E. Vieira dos Santos, F. Souza, C. Saez, P. Cañizares, M.R.V. Lanza, C.A. Martinez-Huitle, M.A. Rodrigo, Application of electrokinetic soil flushing to four herbicides: A comparison, Chemosphere, 153 (2016) 205-211.

[19] J.M. Paz-Garcia, K. Baek, I.D. Alshawabkeh, A.N. Alshawabkeh, A generalized model for transport of contaminants in soil by electric fields, Journal of Environmental Science and Health - Part A Toxic/Hazardous Substances and Environmental Engineering, 47 (2012) 308-318.

605 [20] S.K. Puppala, A.N. Alshawabkeh, Y.B. Acar, R.J. Gale, M. Bricka, Enhanced electrokinetic
606 remediation of high sorption capacity soil, J. Hazard. Mater., 55 (1997) 203-220.
607 [21] K.R. Reddy, U.S. Parupudi, S.N. Devulapalli, C.Y. Xu, Effects of soil composition on the
608 removal of chromium by electrokinetics, J. Hazard. Mater., 55 (1997) 135-158.
609 [22] A.Z. Al-Hamdan, K.R. Reddy, Geochemical assessment of metal transport in glacial till
610 during electrokinetic remediation, Environmental Monitoring and Assessment, 139 (2008) 137-
611 149.
612 [23] A.Z. Al-Hamdan, K.R. Reddy, Transient behavior of heavy metals in soils during
613 electrokinetic remediation, Chemosphere, 71 (2008) 860-871.
614 [24] Y.B. Acar, R.J. Gale, G.A. Putnam, J. Hamed, R.L. Wong, Electrochemical processing of
615 soils: Theory of ph gradient development by diffusion, migration, and linear convection, J.
616 Environ. Sci. Health Part A Environ. Sci. Eng. Toxic Hazard. Subst. Control, 25 (1990) 687-714.
617 [25] P.R. Bloom, U. Skyllberg, Soil pH and pH Buffering, in: P.M. Huang, Y. Li, M.E. Sumner
618 (Eds.) Handbook of Soil Science, CRC Press, USA, 2012, pp. 333-352.
619 [26] R. López-Vizcaíno, A. Yustres, M.J. León, C. Saez, P. Cañizares, M.A. Rodrigo, V. Navarro,
620 Multiphysics Implementation of Electrokinetic Remediation Models for Natural Soils and
621 Porewaters, Electrochimica Acta, 225 (2017) 93-104.
622 [27] C. Risco, R. López-Vizcaíno, C. Sáez, A. Yustres, P. Cañizares, V. Navarro, M.A. Rodrigo,
623 Remediation of soils polluted with 2,4-D by electrokinetic soil flushing with facing rows of
624 electrodes: A case study in a pilot plant, Chem. Eng. J., 285 (2016) 128-136.
625 [28] C. Risco, S. Rodrigo, R. López-Vizcaíno, C. Sáez, P. Cañizares, V. Navarro, M.A. Rodrigo,
626 Electrokinetic flushing with surrounding electrode arrangements for the remediation of soils that
627 are polluted with 2,4-D: A case study in a pilot plant, Sci. Total Environ., 545-546 (2016) 256-
628 265.
629 [29] C. Risco, S. Rodrigo, R. López-Vizcaíno, A. Yustres, C. Sáez, P. Cañizares, V. Navarro,
630 M.A. Rodrigo, Electrochemically assisted fences for the electroremediation of soils polluted with
631 2,4-D: A case study in a pilot plant, Separation and Purification Technology, 156, Part 2 (2015)
632 234-241.
633 [30] R. López-Vizcaíno, V. Navarro, M.J. León, C. Risco, M.A. Rodrigo, C. Sáez, P. Cañizares,
634 Scale-up on electrokinetic remediation: Engineering and technological parameters, J. Hazard.
635 Mater., 315 (2016) 135-143.
636 [31] R. López-Vizcaíno, C. Risco, J. Isidro, S. Rodrigo, C. Saez, P. Cañizares, V. Navarro, M.A.
637 Rodrigo, Scale-up of the electrokinetic fence technology for the removal of pesticides. Part I:
638 Some notes about the transport of inorganic species, Chemosphere, 166 (2017) 540-548.
639 [32] R. López-Vizcaíno, C. Risco, J. Isidro, S. Rodrigo, C. Saez, P. Cañizares, V. Navarro, M.A.
640 Rodrigo, Scale-up of the electrokinetic fence technology for the removal of pesticides. Part II:
641 Does size matter for removal of herbicides?, Chemosphere, 166 (2017) 549-555.
642 [33] C. Risco, S. Rodrigo, R. López Vizcaíno, A. Yustres, C. Saez, P. Cañizares, V. Navarro,
643 M.A. Rodrigo, Removal of oxyfluorfen from spiked soils using electrokinetic soil flushing with
644 linear rows of electrodes, Chem. Eng. J., 294 (2016) 65-72.
645 [34] C. Risco, H. Rubí-Juárez, S. Rodrigo, R. López Vizcaíno, C. Saez, P. Cañizares, C. Barrera-
646 Díaz, V. Navarro, M.A. Rodrigo, Removal of oxyfluorfen from spiked soils using electrokinetic
647 fences, Separation and Purification Technology, 167 (2016) 55-62.
648 [35] C. Risco, H. Rubí-Juárez, S. Rodrigo, R. López-Vizcaíno, C. Saez, P. Cañizares, C. Barrera-
649 Díaz, V. Navarro, M.A. Rodrigo, Removal of oxyfluorfen from spiked soils using electrokinetic
650 soil flushing with the surrounding arrangements of electrodes, Sci. Total Environ., 559 (2016) 94-
651 102.
652 [36] R. López-Vizcaíno, A. Yustres, L. Asensio, C. Saez, P. Cañizares, M.A. Rodrigo, V.
653 Navarro, Enhanced electrokinetic remediation of polluted soils by anolyte pH conditioning,
654 Chemosphere, 199 (2018) 477-485.
655 [37] R. López-Vizcaíno, A. Yustres, C. Sáez, P. Cañizares, M.A. Rodrigo, V. Navarro, Effect of
656 polarity reversal on the enhanced electrokinetic remediation of 2,4-D-polluted soils: A numerical
657 study, Electrochimica Acta, (2017).

[38] Á. Yustres, R. López-Vizcaíno, C. Sáez, P. Cañizares, M.A. Rodrigo, V. Navarro, Water transport in electrokinetic remediation of unsaturated kaolinite. Experimental and numerical study, Separation and Purification Technology, 192 (2018) 196-204.
[39] L.N. Plummer, T.M.L. Wigley, D.L. Parkhurst, Kinetics of calcite dissolution in CO2-water system at 5º to 60ºC and 0.0 to 1. 0 atm CO2, Am J Sci, 278 (1978) 179-216.
[40] W. Stumm, J.J. Morgan, Aquatic chemistry: chemical equilibria and rates in natural waters, Wiley, 1996.
[41] A.C. Lasaga, Kinetic Theory in the Earth Sciences, Princeton University Press, Princeton, NJ, USA, 1998.
[42] N.C.M. Marty, F. Claret, A. Lassin, J. Tremosa, P. Blanc, B. Madé, E. Giffaut, B. Cochepin, C. Tournassat, A database of dissolution and precipitation rates for clay-rocks minerals, Applied Geochemistry, 55 (2015) 108-118.
[43] E. Giffaut, M. Grivé, P. Blanc, P. Vieillard, E. Colàs, H. Gailhanou, S. Gaboreau, N. Marty, B. Madé, L. Duro, Andra thermodynamic database for performance assessment: ThermoChimie, Applied Geochemistry, 49 (2014) 225-236.
[44] A. COMSOL, COMSOL Multiphysics Reference Manual Version: COMSOL 5.1., (2015).
[45] Ö. Babur, V. Smilauer, T. Verhoeff, M. Van Den Brand, A survey of open source multiphysics frameworks in engineering, in: Procedia Computer Science, 2015, pp. 1088-1097.
[46] D.L. Brown, J. Bell, D. Estep, W. Gropp, B. Hendrickson, S. Keller-McNulty, D. Keyes, J.T. Oden, L. Petzold, M. Wright, Applied Mathematics at the U.S. Department of Energy: Past, Present and a View to the Future, Applied Mathematics at the U.S. Department of Energy: Past, Present and a View to the Future, (2008).
[47] D.E. Keyes, L.C. McInnes, C. Woodward, W. Gropp, E. Myra, M. Pernice, J. Bell, J. Brown, A. Clo, J. Connors, E. Constantinescu, D. Estep, K. Evans, C. Farhat, A. Hakim, G. Hammond, G. Hansen, J. Hill, T. Isaac, X. Jiao, K. Jordan, D. Kaushik, E. Kaxiras, A. Koniges, K. Lee, A. Lott, Q. Lu, J. Magerlein, R. Maxwell, M. McCourt, M. Mehl, R. Pawlowski, A.P. Randles, D. Reynolds, B. Rivière, U. Rüde, T. Scheibe, J. Shadid, B. Sheehan, M. Shephard, A. Siegel, B. Smith, X. Tang, C. Wilson, B. Wohlmuth, Multiphysics simulations: Challenges and opportunities, International Journal of High Performance Computing Applications, 27 (2013) 4-83.
[48] J. Carrayrou, R. Mosé, P. Behra, Operator-splitting procedures for reactive transport and comparison of mass balance errors, Journal of Contaminant Hydrology, 68 (2004) 239-268.
[49] D. Jacques, J. Šimůnek, D. Mallants, M.T. van Genuchten, Operator-splitting errors in coupled reactive transport codes for transient variably saturated flow and contaminant transport in layered soil profiles, Journal of Contaminant Hydrology, 88 (2006) 197-218.
[50] J.M. Paz-García, B. Johannesson, L.M. Ottosen, A.N. Alshawabkeh, A.B. Ribeiro, J.M. Rodríguez-Maroto, Modeling of electrokinetic desalination of bricks, Electrochimica Acta, 86 (2012) 213-222.
[51] M.T. van Genuchten, CLOSED-FORM EQUATION FOR PREDICTING THE HYDRAULIC CONDUCTIVITY OF UNSATURATED SOILS, Soil Science Society of America Journal, 44 (1980) 892-898.
[52] D.L. Parkhurst, C.A.J. Appelo, User's guide to PHREEQ C (Version 2) – a computer program for speciation, batch-reaction, one-dimensional transport and inverse geochemical calculations, Water-Resources Investigations, Report 99–4259, Denver, Co, USA, (1999) 312.
[53] M.J. Pikal, Ion-pair formation and the theory of mutual diffusion in a binary electrolyte, The Journal of Physical Chemistry, 75 (1971) 663-675.
[54] M. Villen-Guzman, J.M. Paz-Garcia, G. Amaya-Santos, J.M. Rodriguez-Maroto, C. Vereda-Alonso, C. Gomez-Lahoz, Effects of the buffering capacity of the soil on the mobilization of heavy metals. Equilibrium and kinetics, Chemosphere, 131 (2015) 78-84.
[55] R. López-Vizcaíno, J. Alonso, P. Cañizares, M.J. León, V. Navarro, M.A. Rodrigo, C. Sáez, Electroremediation of a natural soil polluted with phenanthrene in a pilot plant, J. Hazard. Mater., 265 (2014) 142-150.
[56] C.N. Fredd, H. Scott Fogler, The kinetics of calcite dissolution in acetic acid solutions, Chemical Engineering Science, 53 (1998) 3863-3874.

712 [57] A.Z. Al-Hamdan, K.R. Reddy, Electrokinetic remediation modeling incorporating
713 geochemical effects, J. Geotech. Geoenviron. Eng., 134 (2008) 91-105.
714 [58] M.T. van Genuchten, A Closed-form Equation for Predicting the Hydraulic Conductivity of
715 Unsaturated Soils1, Soil Science Society of America Journal, 44 (1980) 892-898.
716 [59] N. Edlefsen, A. Anderson, Thermodynamics of soil moisture, Hilgardia 15 (2) (1943) 31-
717 298.
718 [60] J.K. Mitchell, K. Soga, Fundamentals of soil behavior, John Wiley & Sons, Inc, Hoboken,
719 New Jersey, USA, 2005.
720 [61] R.H. Brooks, A.T. Corey, Hydraulic Properties of Porous Media, Colorado State University,
721 1964.
722 [62] C.M. Bethke, Geochemical and Biogeochemical Reaction Modeling, Cambridge University
723 Press, 2007.
724 [63] A.M.M. Leal, M.J. Blunt, T.C. LaForce, Efficient chemical equilibrium calculations for
725 geochemical speciation and reactive transport modelling, Geochimica et Cosmochimica Acta, 131
726 (2014) 301-322.
727 [64] C.I. Steefel, C.A.J. Appelo, B. Arora, D. Jacques, T. Kalbacher, O. Kolditz, V. Lagneau, P.C.
728 Lichtner, K.U. Mayer, J.C.L. Meeussen, S. Molins, D. Moulton, H. Shao, J. Šimůnek, N. Spycher,
729 S.B. Yabusaki, G.T. Yeh, Reactive transport codes for subsurface environmental simulation,
730 Computational Geosciences, 19 (2015) 445-478.
731 [65] P.C. Lichtner, Continuum model for simultaneous chemical reactions and mass transport in
732 hydrothermal systems, Geochimica et Cosmochimica Acta, 49 (1985) 779-800.
733 [66] R.A. Jacobs, R.F. Probstein, Two-Dimensional Modeling of Electroremediation, AIChE
734 Journal, 42 (1996) 1685-1696.
735 [67] J.D. Rhoades, N.A. Manteghi, P.J. Shouse, W.J. Alves, Soil Electrical Conductivity and Soil
736 Salinity: New Formulations and Calibrations, Soil Science Society of America Journal, 53 (1989)
737 433-439.
738 [68] C.A.J. Appelo, Specific conductance: how to calculate, to use, and the pitfalls, in, 2010.

739

740